Cerebral Cortex, March 2016;26: 977–990

doi: 10.1093/cercor/bhu267
Advance Access Publication Date: 18 November 2014
Original Article

ORIGINAL ARTICLE

Neurotensinergic Excitation of Dentate Gyrus Granule Cells via $G\alpha_q$-Coupled Inhibition of TASK-3 Channels

Haopeng Zhang[1,2,†], Hailong Dong[2,†], Nicholas I. Cilz[1], Lalitha Kurada[1], Binqi Hu[1], Etsuko Wada[3], Douglas A. Bayliss[4], James E. Porter[1], and Saobo Lei[1]

[1]Department of Basic Sciences, School of Medicine and Health Sciences, University of North Dakota, Grand Forks, ND 58203, USA, [2]Department of Anesthesiology, Xijing Hospital, Fourth Military Medical University, Xi'an, Shaanxi Province, People's Republic of China, [3]Department of Degenerative Neurological Diseases, National Institute of Neuroscience, Tokyo, Japan, and [4]Department of Pharmacology, University of Virginia School of Medicine, Charlottesville, VA 22908, USA

Address correspondence to Saobo Lei, Department of Basic Sciences, School of Medicine and Health Sciences, University of North Dakota, Grand Forks, ND 58203, USA. Email: saobo.lei@med.und.edu

[†]H.Z. and H.D. contributed equally to this work.

Abstract

Neurotensin (NT) is a 13-amino acid peptide and serves as a neuromodulator in the brain. Whereas NT has been implicated in learning and memory, the underlying cellular and molecular mechanisms are ill-defined. Because the dentate gyrus receives profound innervation of fibers containing NT and expresses high density of NT receptors, we examined the effects of NT on the excitability of dentate gyrus granule cells (GCs). Our results showed that NT concentration dependently increased action potential (AP) firing frequency of the GCs by the activation of NTS1 receptors resulting in the depolarization of the GCs. NT-induced enhancement of AP firing frequency was not caused indirectly by releasing glutamate, GABA, acetylcholine, or dopamine, but due to the inhibition of TASK-3 K^+ channels. NT-mediated excitation of the GCs was G protein dependent, but independent of phospholipase C, intracellular Ca^{2+} release, and protein kinase C. Immunoprecipitation experiment demonstrates that the activation of NTS1 receptors induced the association of $G\alpha_{q/11}$ and TASK-3 channels suggesting a direct coupling of $G\alpha_{q/11}$ to TASK-3 channels. Endogenously released NT facilitated the excitability of the GCs contributing to the induction of long-term potentiation at the perforant path-GC synapses. Our results provide a cellular mechanism that helps to explain the roles of NT in learning and memory.

Key words: channel, depolarization, glutamate, hippocampus, memory, peptide, synapse, synaptic transmission

Introduction

Neurotensin (NT) is a tridecapeptide initially isolated from bovine hypothalamus (Carraway and Leeman 1973). NT interacts with 3 subtypes of NT receptors: NTS1, NTS2, and NTS3. NTS1 and NTS2 are G protein-coupled receptors, whereas NTS3 is part of the Vps10p family of sorting receptors containing a single transmembrane domain that mainly localizes intracellularly (Hermans and Maloteaux 1998; Mazella et al. 1998; Nouel et al. 1999; Mazella 2001; Pelaprat 2006). NTS1 has high affinity for NT, and its effects are blocked by the selective nonpeptide antagonist SR48692, but insensitive to the antihistamine drug, levocabastine (Vincent et al. 1999; Pelaprat 2006; St-Gelais et al. 2006).

NTS1 is mainly coupled to phospholipase C (PLC) and the inositol phosphate signaling cascade via G_q proteins (Watson et al. 1992). NTS2 shares only about 40% amino acid identity with NTS1, shows lower affinity for NT, and is sensitive to levocabastine (Pelaprat 2006). Different from NTS1, the pharmacological and signaling properties of NTS2 are still controversial and it is still uncertain as to whether NT is an agonist, inverse agonist, or antagonist for this receptor type (Mazella et al. 1996; Sarret et al. 2002; Hwang et al. 2009). To date, very little is known about the physiological role of NTS3 receptors, and they may be involved in molecule sorting between the cell surface and intracellular compartments (Mazella 2001; Navarro et al. 2001).

NT is widely distributed in the periphery such as the gastrointestinal tract and many brain regions including the hippocampus (Roberts et al. 1981; Kohler et al. 1985; Sakamoto et al. 1986; Alexander et al. 1989; Lotstra et al. 1989). Furthermore, the binding sites for NT have also been detected in the hippocampus (Quirion et al. 1987; Boudin et al. 2000) and dentate gyrus (Kohler et al. 1987; Moyse et al. 1987; Cadet et al. 1993; Rowe et al. 2006). Whereas the expressions of both NT and NT receptors in the hippocampus suggest a role for NT in this subcortical structure, the exact functions of NT in this brain region have not been determined. This issue is likely to be important because the hippocampus is a critical structure involved in learning and memory, and there is convincing evidence demonstrating that NT modulates cognitive processes. For instance, variance in working memory performance is closely associated with NTS1 polymorphisms among adult humans (Li et al. 2011); NT binding sites are varied as a function of age and cognitive status (Rowe et al. 2006); application of NT receptor agonists in vivo enhances (Azmi et al. 2006; Ohinata et al. 2007; Laszlo et al. 2010; Xiao et al. 2014), whereas application of NT receptor antagonists hinders (Tirado-Santiago et al. 2006; Laszlo et al. 2010) cognitive functions; whereas the effects of NT on memory are usually considered to be mediated by NTS1 (Azmi et al. 2006; Tirado-Santiago et al. 2006; Ohinata et al. 2007; Laszlo et al. 2010; Xiao et al. 2014), reduced fear memory has also been observed in NTS2 knockout (KO) mice (Yamauchi et al. 2007). Here, we examined the effects of NT on neuronal excitability of the dentate gyrus granule cells (GCs). We chose the GCs for our study because of the following reasons. First, the binding sites for NT have been detected in the dentate gyrus (Kohler et al. 1987; Moyse et al. 1987; Cadet et al. 1993; Rowe et al. 2006). Second, a very large population of NT-containing cell bodies was observed in the entorhinal cortex (Atoji et al. 1995) and the axons of the neurons in layer II of the entorhinal cortex form the perforant path (PP) that innervates the dentate gyrus. Third, numerous NT-immunoreactive varicose axons have been detected in the molecular layer of the dentate gyrus (Sakamoto et al. 1986), where the PP arrives. These results suggest that endogenously released NT exerts potential actions in the dentate gyrus. Our results demonstrate that NT transiently increased the neuronal excitability of the GCs by inhibiting TASK-3 channels. NT-mediated increases in neuronal excitability facilitate long-term potentiation (LTP) at the PP-GC synapses.

Materials and Methods

Slice Preparation

The ages of the animals used for electrophysiological recordings were postnatal 14–20 days for Sprague–Dawley rats, individual KO and their corresponding wild-type (WT, C57BL/6J) mice. Experimental procedures for breeding and genotyping of NTS1, NTS2 (Maeno et al. 2004), or TASK-3 (Lazarenko et al. 2010) KO mice were described previously. Horizontal brain slices (400 μm) were prepared from rats or mice as described previously (Wang et al. 2011, 2012; Ramanathan et al. 2012). All animal procedures conformed to the guidelines approved by the University of North Dakota Animal Care and Use Committee.

Recordings of Action Potentials by Perforated Patches

Because the dentate gyrus GCs could not sustain continuous firing in whole-cell recording configuration, we used perforated patch-clamp configuration to record action potentials (APs), as described previously (Deng and Lei 2007; Deng et al. 2010). Slices were perfused with the normal extracellular solution comprised (in mM) 130 NaCl, 24 $NaHCO_3$, 3.5 KCl, 1.25 NaH_2PO_4, 2.5 $CaCl_2$, 1.5 $MgCl_2$, and 10 glucose, saturated with 95% O_2 and 5% CO_2 (pH 7.4). To exclude potential influences of NT-induced alterations of synaptic transmission on AP firing frequency, we included in the above-mentioned normal extracellular solution (in μM) 10 DNQX, 50 DL-APV, 10 bicuculline, and 2 CGP55845 to block AMPA/kainate, NMDA, $GABA_A$, and $GABA_B$ receptors, respectively. Recording pipettes were tip-filled with the solution containing (in mM) 100 K^+-gluconate, 0.6 EGTA, 2 $MgCl_2$, 8 NaCl, 33 HEPES, 2 $ATPNa_2$, 0.4 GTPNa, and 7 phosphocreatine (pH 7.4) and then back-filled with freshly prepared K^+-gluconate intracellular solution containing amphotericin B (200 μg/ml, Calbiochem). Patch pipettes had resistance of 6–8 MΩ when filled with the preceding solution. A 5-mV hyperpolarizing test pulse was applied every 3 s to monitor the changes of the series resistance and the process of perforation. Stable series resistances (50–70 MΩ) were usually obtained ~30 min after the formation of gigaohm seals. For those cells showing abrupt reduction in series resistance during membrane perforation suggesting the simultaneous formation of whole-cell configuration, experiments were terminated immediately. Perforated-patch configurations were verified by examining the series resistance again at the end of the experiments. Data were included for analysis only from those cells showing <15% alteration of series resistance. For recordings of APs, a positive current injection was required to bring the membrane potential to ~ −50 mV to induce AP firing. Data were filtered at 2 kHz, digitized at 10 kHz and acquired using pCLAMP 9 or pCLAMP 10 software (Molecular Devices). The recorded APs were analyzed afterward using Mini Analysis 6.0.1 (Synaptosoft, Inc.). NT was dissolved in the extracellular solution and applied to the cells. Only one cell was recorded from each slice to exclude NT-induced desensitization. For experiments involving inhibitors for individual molecules, slices were pretreated with individual inhibitors for at least 2 h, and the bath was continuously perfused with the same concentration of the inhibitors during the experiments unless stated otherwise.

Recordings of Holding Currents and Resting Membrane Potentials by Whole-Cell Patch-Clamp Recordings

Holding currents (HCs) at −60 mV and resting membrane potentials (RMPs) were recorded in the above-mentioned normal extracellular solution supplemented with 0.5 μM tetrodotoxin (TTX) to block AP firings and synaptic transmission. I–V curves were constructed in the normal extracellular solution supplemented with (in μM) 10 DNQX, 50 DL-APV, 10 bicuculline, 2 CGP55845, 0.5 TTX, 100 $CdCl_2$, and 100 $NiCl_2$ to block synaptic transmission, Na^+, and Ca^{2+} channels. I–V curves were obtained by using a ramp protocol from −120 to −60 mV at a rate of 0.03 mV/ms. We compared the I–V curves recorded prior to and during the application of NT for 4–7 min at which the maximal effect of NT was observed.

Recordings of LTP at the PP-GC Synapses

Whole-cell recordings were used to record LTP from the GCs. The intracellular solution was the above K^+-gluconate internal solution unless stated otherwise. The above-mentioned normal extracellular solution was supplemented with 10 μM bicuculline and 2 μM CGP55845 to block GABAergic transmission. PP was stimulated by placing a concentric bipolar stimulation electrode (FHC, MX21XES(DB9)) in the middle to the inner one-third of the molecular layer of the dentate gyrus to stimulate the medial PP. The stimulation intensity was set to the level that produced 30–40% of the maximal amplitude of EPSCs. After recording basal AMPA EPSCs in voltage-clamp mode for 5–10 min, we applied an induction protocol (100 Hz for 1 s, repeated for 5 times at an interval of 10 s) in current-clamp mode with the same stimulation intensity to induce LTP. A positive current was injected to bring the membrane potential to ~−50 mV during the application of the induction protocol. Immediately after the induction protocol, AMPA EPSCs were recorded again in voltage-clamp mode to monitor the expression of LTP. The amplitudes of AMPA EPSCs were normalized to the average of those recorded in control condition for 5 min.

Expression of NTS1 and TASK-3 Channels in HEK293 Cells and Electrophysiological Recordings from the Transfected Cells

Detailed methods for transfection and electrophysiological recordings from the transfected cells were described previously (Deng et al. 2007, 2009; Xiao et al. 2009; Xiao et al. 2014). Briefly, cDNA constructs coding for human NTS1 receptors (GenBank accession number AY429106, subcloned into pCDNA3.1 vector) was obtained from the Missouri S&T cDNA Resource Center (www.cdna.org). cDNA constructs coding for rat N-terminal GFP-tagged TASK-3 (GenBank Accession Number AF391084, subcloned into pEGFP vector, Clontech) were used as previously described (Berg et al. 2004; Deng et al. 2009). HEK293 cells obtained from American Type Culture Collection were maintained in DMEM containing 10% FBS, penicillin (100 U/ml), and streptomycin (100 U/ml). Confluent HEK293 cells were washed in Hank's Balance Salt Solution, trypsinized, and seeded at the appropriate density in 35-mm dishes to ensure 50–80% cell confluence within 24 h. HEK293 cells were transfected with NTS1 alone, TASK-3 channels alone, or NTS1 together with TASK-3 channels. Transient transfection of the cDNA constructs was performed after 24 h with GeneJammer transfection reagent according to the manufactures protocol (Agilent Technologies) using a 6 μl reagent per 2 μg cDNA ratio for the transfection cocktail. Transfected HEK293 cells were subsequently used for electrophysiological recordings 24–36 h post-transfection.

HCs at −60 mV were recorded from the HEK293 cells that showed fluorescence under a fluorescence microscope (Olympus 1X70) by whole-cell recordings. The extracellular solution contained (in mM) 130 NaCl, 3 KCl, 2 $MgCl_2$, 2 $CaCl_2$, 1.25 NaH_2PO_4, 10 HEPES, and 10 glucose (pH 7.4 adjusted with NaOH and HCl). The above-mentioned K^+-gluconate internal solution was used for this experiment. A continuous gravity perfusion system (flow, 5–7 mL/min) was used to change solutions.

Immunocytochemistry

Detailed procedures for immunocytochemistry were described previously (Deng et al. 2009; Xiao et al. 2009; Ramanathan et al. 2012). Sprague–Dawley rats (18 days, $n = 4$), WT mice (32 days, $n = 3$), and NTS1 KO mice (31 days, $n = 3$) were deeply anesthetized with pentobarbital sodium (50 mg/kg) and then perfused transcardially with physiological saline followed by 4% (v/v) ice-cold paraformaldehyde in PBS (pH = 7.4). Brains were post-fixed for 6–8 h in the same fixative at 4°C and cryoprotected in 15% (w/v) and 30% (w/v) sucrose solutions. Coronal sections (10 μm) were cut on a freezing microtome (Leica CM3050 S). After blocking with PBS containing 0.3% (v/v) Triton X-100 and 10% (v/v) normal donkey serum, sections were incubated overnight at 4°C with primary antibodies for the neuronal nuclei marker (NeuN, rabbit monoclonal antibody, 1:2000, Chemicon) and NTS1 (goat polyclonal antibody, 1:300, sc-7596, Santa Cruz Biotechnology). The sections were washed with PBS and incubated with the secondary antibody solution containing Texas Red-labeled donkey anti-goat antibody (IgG, 1:500, sc-2781, Santa Cruz Biotechnology) and FITC-labeled goat anti-rabbit antibody (IgG, 1:500, sc-2012, Santa Cruz Biotechnology) at room temperature for 2 h. Finally, sections were observed, and images were captured using a fluorescence microscope (Leica DM5000 B). For a control, the NTS1 antibody was pre-adsorbed with the specific blocking peptide (sc-7596P, Santa Cruz Biotechnology) before being applied to the tissue sections and the other procedures were the same.

Immunoprecipitation and Western Blot

Horizontal brain slices were cut initially from Sprague–Dawley rats, WT, and TASK-3 KO mice ($n = 6$ for each species). The dentate gyrus region was punched out from the slices under a microscope. The isolated dentate gyrus region was treated with or without 0.5 μM NT in the oxygenated extracellular solution for 5 min. Tissue lysates were then prepared as described previously (Deng et al. 2009; Xiao et al. 2009, 2014). The lysates were centrifuged at 14 000 rpm for 10 min to remove insoluble materials, and protein concentration in the supernatant was determined (Bradford 1976). An equivalent protein was added to Eppendorf tubes. TASK-3 channels from these slices were immunoprecipitated using goat TASK-3 antibody (1 μg antibody/mg protein; sc-11317, Santa Cruz Biotechnology) by overnight rocking at 4°C. Protein was then added to agarose beads (40 μL beads/immunoprecipitation, Protein A/G PLUS–Agarose, Santa Cruz Biotechnology) and rocked at 4°C for 2 h. Beads were spun down, and the buffer was aspirated. Beads were then rinsed with cold RIPA buffer for 3–5 times. Equal amount of sample buffer was added to the beads and then boiled for 5 min at 95°C. The immunoprecipitates were resolved by SDS–PAGE and western-blotted with rabbit $G\alpha_{q/11}$ antibody (1:500, 371 751, Calbiochem) and goat anti-rabbit IgG-HRP (1:5000, sc-2004, Santa Cruz Biotechnology). Donkey anti-goat HRP conjugate (1:5000, sc-2020, Santa Cruz Biotechnology) was used to probe TASK-3 (1:500, sc-11317, Santa Cruz Biotechnology). Immunoreactive bands were visualized by SuperSignal West Pico Chemiluminescent Substrate (Pierce) and detected by a Biospectrum Imagining System (UVP). Detailed methods for western blot were described previously (Xiao et al. 2009, 2014).

Data Analysis

Data are presented as the means ± SEM. Concentration–response curve for NT was fit by Hill equation: $I = I_{max} \times \{1/[1 + (EC_{50}/[ligand])^n]\}$, where I_{max} is the maximum response, EC_{50} is the concentration of ligand producing a half-maximal response, and n is the Hill coefficient. We fit the net I–V curve induced by

NT with the Goldman–Hodgkin–Katz (GHK) current equation:

$$I_s = P_s z_s \frac{EF^2}{RT} \frac{[S]_i - [S]_o \exp(-z_s FE/RT)}{1 - \exp(-z_s FE/RT)},$$

where P_s is the permeability, $[S]_i$ and $[S]_o$ are the intracellular and extracellular concentrations of potassium, z_s is the valence, F is Faraday's constant, R is the gas constant, E is the voltage and T is the absolute temperature. Student's paired or unpaired t test or analysis of variance (ANOVA) was used for statistical analysis as appropriate; P-values are reported throughout the text and significance was set as $P < 0.05$. For the analysis of the time course of AP firing frequency, data recorded from each neuron were normalized to the average of the firing frequency in 5 min prior to the application of NT. N number in the text represents the cells examined.

Chemicals

NT, NT1-8 and NT8-13 were provided by American Peptide Company. The following reagents were purchased from TOCRIS: MCPG, SCH23390, sulpiride, SR48692, tertiapin-Q, ruthenium red, GDP-β-S, U73122, xestospongin C, BAPTA, and GF109203X. Edelfosine was purchased from Calbiochem. Anti-$G_{\alpha q/11}$ (catalog No., 371 751) was bought from Calbiochem. Anti-G_{β} (T-20, sc-378) was the product of Santa Cruz Biotechnology, Inc. Levocabastine, PD149163, bupivacaine, atropine, and mecamylamine were products of Sigma–Aldrich.

Results

NT Transiently Increases AP Firing Frequency in the GCs

We used amphotericin B-perforated patches to record stable AP firing from the dentate gyrus GCs. Bath application of NT (0.5 μM) for 5 min significantly increased the firing frequency of APs (343 ± 56% of control, $n = 7$, $P = 0.005$, Fig. 1A,B). NT-induced increases in AP firing frequency were reversible after wash in NT-free extracellular solution for 20 min (116 ± 22% of control, $n = 7$, $P = 0.49$ vs. baseline, Fig. 1A,B). The EC_{50} of NT to increase AP firing frequency was calculated to be 0.22 μM (Fig. 1C). We applied 0.5 μM NT for the remaining experiments because this is a near saturating NT concentration. The effect of NT on AP firing was likely mediated by the activation of NT receptors because bath application of the active fragment, NT8-13 (0.5 μM), exerted the same action as NT (322 ± 73% of control, $n = 9$, $P = 0.016$, Fig. 1D) but application of the inactive fragment, NT1-8 (0.5 μM), had no effects on AP firing (103 ± 3% of control, $n = 5$, $P = 0.49$, Fig. 1D).

Whereas NT has been reported to modulate the release of glutamate (Yin et al. 2008; Kadiri et al. 2011) and GABA (O'Connor et al. 1992; Rakovska et al. 1998; Li et al. 2008; Petkova-Kirova et al. 2008) in some brain regions, NT-induced increases in AP firing frequency were unlikely to be mediated by glutamate or GABA because the extracellular solution contained blockers for glutamate (DNQX and DL-APV) and GABA (bicuculline and CGP55845) receptor (see Materials and Methods). Inclusion of MCPG (1 mM), a broad-spectrum metabotropic glutamate receptor (mGluR) antagonist, in the extracellular solution failed to alter NT-induced augmentation of AP firing frequency (390 ± 52% of control, $n = 7$, $P = 0.89$ vs. NT alone, Fig. 2A), excluding the involvement of mGluRs. NT has also been reported to modulate the release of acetylcholine (Lapchak et al. 1990, 1991; Rakovska et al. 1998; Petkova-Kirova et al. 2008) and dopamine (Faggin et al. 1990; Reyneke et al. 1992), and NT receptors may

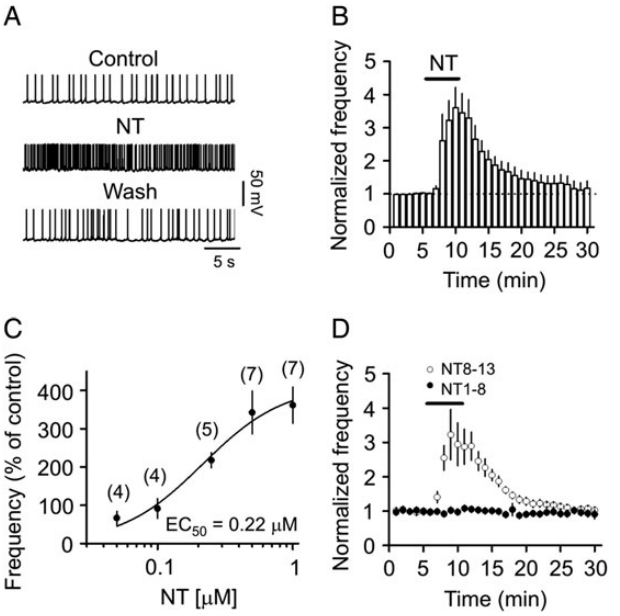

Figure 1. NT transiently increases the AP firing frequency of dentate gyrus GCs assessed by perforated patches. (*A*) APs recorded from a dentate gyrus GC before, during, and after the application of NT (0.5 μM). (*B*) Time course of AP firing frequency pooled from 7 cells. (*C*) Concentration–response curve of NT. The numbers in the parentheses were numbers of cells recorded at each concentration. (*D*) Bath application of the active fragment of NT (NT8-13) at the concentration of 0.5 μM transiently enhanced the AP firing frequency, whereas application of the inactive fragment (NT1-8) at the same concentration failed to augment the AP firing frequency.

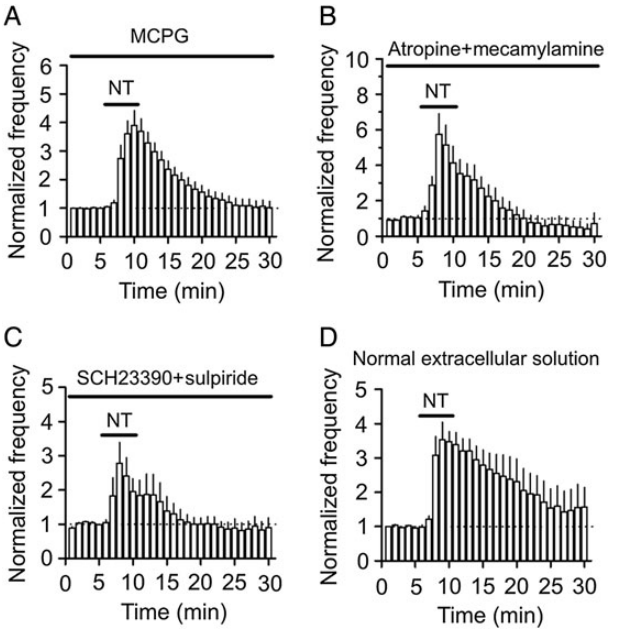

Figure 2. NT-induced augmentation of AP firing frequency is not mediated by the activation of mGluRs, acetylcholine, and dopamine receptors. (*A*) Application of mGluRs antagonist, MCPG, did not block NT-induced increases in AP firing frequency. (*B*) NT still increased AP firing frequency in the presence of antagonists to muscarinic (atropine) and nicotinic (mecamylamine) receptors. (*C*) Blockade of dopamine D_1-like and D_2-like receptors, respectively, by SCH23390 and sulpiride failed to block NT-induced enhancement of AP firing frequency. (*D*) Application of NT in the extracellular solution without any antagonists still induced an increase in AP firing frequency.

interact with dopamine receptors in some brain regions (von Euler et al. 1989; Ferraro et al. 1997; Diaz-Cabiale et al. 2002; Amano et al. 2008). Application of atropine (10 μM, a muscarinic receptor antagonist) and mecamylamine (100 μm, a nicotinic receptor antagonist) failed to change NT-induced enhancement of AP firing frequency (575 ± 117% of control, $n = 7$, $P = 0.92$ vs. NT alone, Fig. 2*B*) suggesting that it is unlikely that NT facilitates neuronal excitability via releasing acetylcholine. In the same fashion, application of SCH23390 (10 μM, a D_1-like receptor antagonist) and sulpiride (100 μM, a D_2-like receptor antagonist) did not alter NT-induced increases in AP firing frequency (278 ± 61% of control, $n = 7$, $P = 0.28$ vs. NT alone, Fig. 2*C*). These results together indicate that NT-induced increases in AP firing frequency are not mediated indirectly by modulating the release of acetylcholine and dopamine. Finally, application of NT in the pure extracellular solution without any receptor antagonists still increased AP firing frequency (354 ± 50% of control, $n = 6$, $P = 0.004$, Fig. 2*D*), supporting the notion that NT facilitates AP firing frequency in normal physiological conditions.

NT-Induced Increase in AP Firing Frequency is Mediated by Activation of NTS1 Receptors

We then characterized the NT receptor subtype facilitating AP firing frequency. Application of the selective NTS1 antagonist, SR48692 (1 μM), significantly reduced NT-induced augmentation of AP firing frequency (115 ± 4% of control, $n = 5$, $P = 0.02$ vs. control without SR48692, two-way ANOVA, Fig. 3A_1,A_2), suggesting that NT increases AP firing frequency via the activation of NTS1 receptors. Furthermore, bath application of the selective NTS1 agonist, PD149163 (0.5 μM), significantly augmented the frequency of AP firing (152 ± 8% of control, $n = 6$, $P = 0.001$, Fig. 3B_1,B_2), further confirming the involvement of NTS1 receptors. However, application of levocabastine (30 μM), a selective NTS2 antagonist, failed to block NT-mediated facilitation of AP firing (418 ± 68% of control, $n = 5$, $P = 0.01$, Fig. 3C_1,C_2) suggesting that NTS2 receptors are not required for NT-induced increases in AP firing. We further explored the roles of NT receptors by using NT receptor KO mice. Bath application of NT to slices cut from NTS1 KO mice failed to enhance AP firing frequency (103 ± 3% of control, $n = 11$ cells from 3 mice, $P = 0.38$, Fig. 3D_1,D_2) whereas the application of NT still increased the frequency of AP firing in slices cut from NTS2 KO mice (288 ± 25% of control, $n = 12$ cells from 4 mice, $P < 0.001$, Fig. 3E_1, E_2). Consistent with our electrophysiological data, immunostaining experiments detected a high density of NTS1 receptor immunoreactivity in the dentate gyrus GCs of the rats and WT mice but not in those of NTS1 KO mice (Fig. 3*F*).

NT Induces Membrane Depolarization via Inhibition of K^+ Channels

NT could facilitate AP firing frequency by generating membrane depolarization. We therefore measured the alterations of RMPs and input resistance in response to bath application of NT in the extracellular solution containing TTX to block AP firing. Application of NT induced depolarization of GCs (control: −65.5 ± 1.3 mV, NT: −58.8 ± 2.2 mV, $n = 7$, $P < 0.001$, Fig. 4*A*,*B*). As demonstrated previously (Ambrogini et al. 2004), the input resistance of granule cells varied significantly (Fig. 4*C*) and application of NT slightly but significantly increased the input resistance (control: 774 ± 107 MΩ; NT: 823 ± 100 MΩ, $n = 7$, $P = 0.01$, Fig. 4*C*). We also recorded the HCs in voltage clamp. NT induced a small inward HC (−12.1 ± 1.9 pA, $n = 5$, $P = 0.003$, Fig. 4*D*). These results demonstrate that NT increases AP firing frequency by generating membrane depolarization.

We then determined the ionic mechanisms underlying NT-mediated increases in AP firing frequency by monitoring NT-induced changes of RMP. When K^+-gluconate was included in the pipettes, bath application of NT induced a depolarization with a net voltage change of 5.0 ± 0.9 mV ($n = 8$, $P < 0.001$, Fig. 4*E*,*J*). We first tested whether NT generated membrane depolarization by opening a cationic conductance. If so, influx of extracellular Na^+ should be the major ion to mediate membrane depolarization. We therefore replaced extracellular NaCl with the same concentration of NMDG-Cl. In this situation, bath application of NT still induced a comparable depolarization (3.9 ± 0.5 mV, $n = 6$, $P = 0.34$ vs. NT alone, Fig. 4*F*,*J*), suggesting that NT-induced depolarization is not mediated by Na^+ influx. We next tested whether extracellular Ca^{2+} is necessary for NT-induced depolarization. Replacement of extracellular Ca^{2+} with the same concentration of Mg^{2+} and inclusion of 1 mM EGTA in the extracellular solution did not significantly alter NT-induced depolarization (4.2 ± 0.6 mV, $n = 5$, $P = 0.49$ vs. NT alone, Fig. 4*G*,*J*), suggesting that extracellular Ca^{2+} is unnecessary for NT-induced depolarization. These results together demonstrate that NT-induced depolarization is not mediated by opening a cationic conductance.

NT has been reported to inhibit Na^+/K^+ pump (Lopez Ordieres and Rodriguez de Lores Arnaiz 2000). This pump creates a concentration gradient by moving 3 Na^+ out of the cells and 2 K^+ into the cells. Inhibition of the Na^+/K^+ pump results in a net accumulation of positive ions inside the cells leading to depolarization. We therefore tested this mechanism by replacing extracellular K^+ with the same concentration of Na^+ to inactivate the Na^+/K^+ pump. In this condition, application of NT induced an even larger depolarization (8.7 ± 1.0 mV, $n = 9$, $P = 0.018$ vs. NT alone, Fig. 4*H*,*J*) suggesting that NT-induced depolarization was not through the inhibition of the Na^+/K^+ pump. One explanation for the significant larger depolarization induced by NT in the absence of extracellular K^+ may be that depletion of extracellular K^+ increased the driving force for K^+ efflux via K^+ channels and hence facilitated the depolarizing effect of NT (see below).

We next tested the roles of K^+ channels by replacing intracellular K^+-gluconate with Cs^+-gluconate. In this situation, bath application of NT failed to significantly induce depolarization (0.4 ± 0.3 mV, $n = 5$, $P = 0.17$ vs. baseline, $P = 0.002$ vs. NT alone, Fig. 4*I*,*J*). These results suggest that NT-mediated depolarization is mediated via the inhibition of K^+ channels.

If K^+ channels are involved, the net current generated by NT should have a reversal potential close to the K^+ reversal potential. We therefore measured the reversal potential of the NT-generated net currents using a ramp protocol (Fig. 4*K*). The net current generated by NT had a reversal potential of −85.8 ± 1.7 mV ($n = 6$, Fig. 4*L*), which is close to the calculated K^+ reversal potential (−85.5 mV). NT-generated net current could be fit by GHK equation (Fig. 4*L*), suggesting the involvement of TASK-like channels (see below).

Activation of NTS1 Receptors Inhibits TASK-3 Channels

We then tested the effects of Ba^{2+}, a K^+ channel blocker, on NT-induced depolarization. Application of Ba^{2+} (3 mM) alone induced remarkable depolarization (10.1 ± 1.4 mV, $n = 6$, $P < 0.001$, Fig. 5*A*), and subsequent application of NT in the presence of Ba^{2+} failed to further alter the membrane potential significantly (0.3 ± 0.3 mV, $n = 6$, $P = 0.43$, Fig. 5*A*,*J*). Because the inward rectifier K^+ channels (Kir) are sensitive to Ba^{2+}, we used 2 Kir inhibitors, SCH23390 (Kuzhikandathil and Oxford 2002) and tertiapin-Q, to further

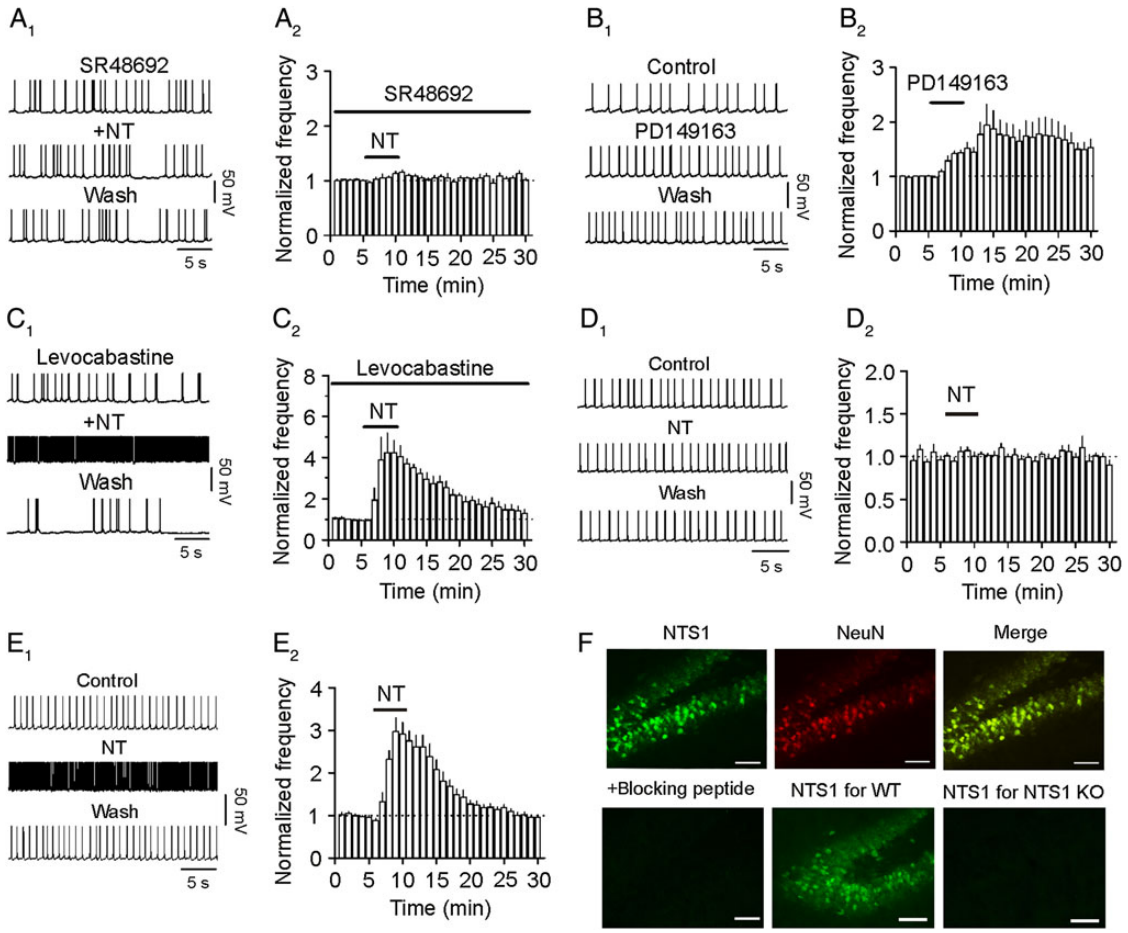

Figure 3. NT increases AP firing frequency via the activation of NTS1 receptors. (A_1,A_2) Application of the NTS1 antagonist, SR48692 (1 μM), almost completely blocked NT-induced facilitation of AP firing frequency. (A_1) APs recorded before, during, and after the application of NT in the presence of SR48692. (A_2) Pooled time course of the AP firing frequency in response to NT in the presence of SR48692. Data were shown in the same fashion thereafter. (B_1,B_2) Bath application of the NTS1 agonist, PD149163 (0.5 μM), significantly increased AP firing frequency. (C_1,C_2) Pretreatment of slices with and continuous bath application of the NTS2 antagonist, levocabastine (30 μM), did not alter significantly NT-induced transient enhancement of AP firing frequency. (D_1,D_2) Bath application of NT to slices cut from NTS1 KO mice failed to augment AP firing frequency. (E_1,E_2) Bath application of NT to slices cut from NTS2 KO mice still augmented AP firing frequency. (*F*) The dentate gyrus expressed NTS1 receptors. Upper left: immunostaining for NTS1 in the dentate gyrus GCs of rats; upper middle: immunostaining for the specific neuronal marker, NeuN, in rats; upper right: merged micrograph to show the expression of NTS1 in the dentate gyrus GCs of rats; lower left: no immunoreactivity was detected in the dentate gyrus of rats when NTS1 antibody was pre-adsorbed with the specific blocking peptide. Lower middle: immunostaining for NTS1 in the dentate gyrus GCs of WT mice. Lower right: no immunoreactivity was detected in the dentate gyrus GCs of NTS1 KO mice. Scale bar: 50 μm.

probe their roles in NT-induced depolarization. NT still induced comparable depolarization in the presence of SCH23390 (20 μM, 4.9 ± 0.8 mV, $n = 11$, $P = 0.9$ vs. NT alone, Fig. 5*B*,*J*) or tertiapine-Q (0.5 μM, 4.5 ± 1.1 mV, $n = 6$, $P = 0.7$ vs. NT alone, Fig. 5*C*,*J*). These data excluded the involvement of Kirs. Because TASK channels are also sensitive to Ba^{2+} (Bayliss et al. 2003; Lesage 2003), we examined the roles of TASK channels in NT-induced depolarization. TASK channels are sensitive to acid and bupivacaine (Bayliss et al. 2003). We thus tested the effects of pH and bupivacaine on NT-induced depolarization. Lowering the extracellular pH from 7.3 to 6.5 induced a significant depolarization (4.8 ± 0.7 mV, $n = 6$, $P < 0.001$, Fig. 5*D*), and subsequent application of NT failed to further alter membrane depolarization (1.0 ± 0.6 mV, $n = 6$, $P = 0.13$, Fig. 5*D*,*J*). Similarly, bath application of bupivacaine (200 μM) induced remarkable depolarization (5.8 ± 0.7 mV, $n = 6$, $P < 0.001$, Fig. 5*E*) and blocked NT-induced depolarization (1.1 ± 0.5 mV, $n = 6$, $P = 0.06$, Fig. 5*E*,*J*) further supporting the involvement of TASK channels. Because the dentate gyrus GCs express a high density of TASK-3 channels (Talley et al. 2001), we next tested the role of TASK-3 channels in NT-induced depolarization by applying 2 TASK-3 channel blockers, zinc, and ruthenium red (Bayliss et al. 2003). Application of zinc and ruthenium red by themselves induced significant depolarization (zinc: 3.1 ± 0.3 mV, $n = 7$, $P < 0.001$, Fig. 5*F*; ruthenium red: 2.9 ± 0.4 mV, $n = 5$, $P = 0.002$, Fig. 5*G*). NT-induced depolarization was significantly reduced by zinc (1.0 ± 0.3 mV, $n = 7$, $P = 0.001$ vs. NT alone, Fig. 5*F*,*J*) and blocked by ruthenium red (0.8 ± 0.6 mV, $n = 5$, $P = 0.24$ vs. baseline, Fig. 5*G*,*J*), suggesting the involvement of TASK-3 channels. We further confirmed the role of TASK-3 channels by using TASK-3 KO mice (Lazarenko et al. 2010). The RMPs of the dentate gyrus GCs in slices cut from the TASK-3 KO mice (–69.3 ± 1.4 mV, $n = 10$ cells from 3 mice) were not significantly different from those recorded from WT mice (–70.3 ± 1.4 mV, $n = 9$ cells from 3 mice, $P = 0.62$, data not shown). One possible explanation is that the roles of TASK-3 channels may be replaced by other K^+ channels in TASK-3 KO mice as observed in TASK-1 (Aller et al. 2005), TREK-1 (Heurteaux et al. 2004), and TREK-2 (Xiao et al. 2014) KO mice. Application of NT induced a significantly smaller level of depolarization in slices

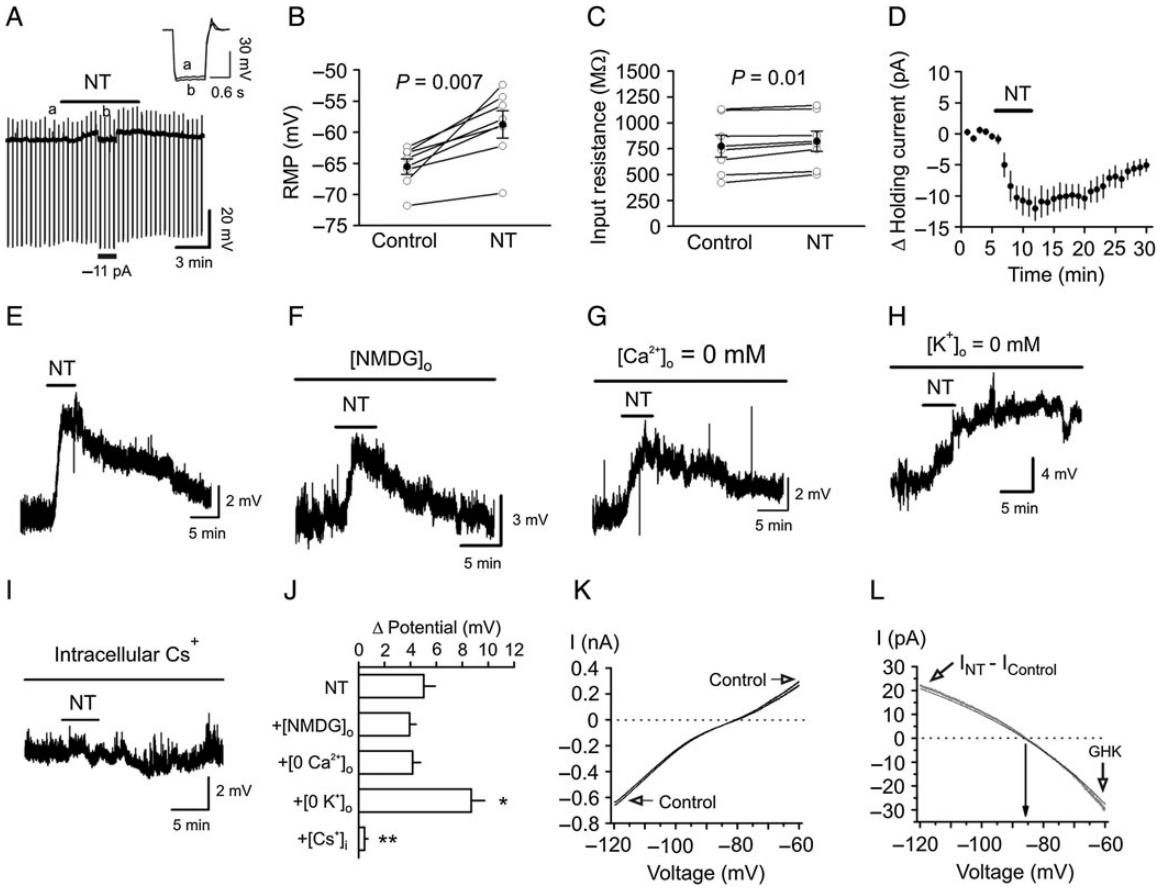

Figure 4. NT-mediated enhancement of neuronal excitability is mediated by inhibiting a background K^+ channel. (*A*) Bath application of NT generated membrane depolarization and slightly increased the input resistance of the GCs. RMP was recorded in current-clamp mode, and a hyperpolarizing current (−50 pA, 500 ms) was injected every 20 s to measure the input resistance. Note that NT generated depolarization and slightly increased the input resistance. To exclude the influence of NT-induced membrane depolarization on the input resistance, a negative current (−11 pA indicated by the horizontal bar) was injected briefly to bring the membrane potential back to the initial level. Inset is the voltage traces taken before (a) and during (b) the application of NT when the negative current was injected. (*B*) Pooled RMPs from 7 cells before and during the application of NT. (*C*) Pooled input resistance from 7 cells before and during the application of NT. (*D*) Application of NT induced an inward HC. (*E*) NT induced membrane depolarization recorded in current clamp from a GC. (*F*) Replacement of extracellular NaCl with NMDG-Cl did not block NT-induced depolarization. (*G*) Substitution of extracellular Ca^{2+} with Mg^{2+} and inclusion of EGTA (1 mM) in the extracellular solution failed to annul NT-induced depolarization. (*H*) NT induced an even larger depolarization in the absence of extracellular K^+. (*I*) Bath application of NT failed to induce depolarization when Cs^+-gluconate was included in the recording pipette. (*J*) Summary bar graph. $^*P < 0.05$, $^{**}P < 0.01$ vs. NT alone. (*K*) I–V curves recorded by a ramp protocol (from −120 to −60 mV) in the extracellular solution containing 3.5 mM K^+ before and during the application of NT. (*L*) The NT-generated net current obtained by subtraction of the control from that in the presence of NT could be fit by GHK equation.

cut from TASK-3 KO mice (1.4 ± 0.2 mV, $n = 10$ cells from 3 mice, $P < 0.001$ vs. baseline) than that recorded in slices cut from WT mice (3.9 ± 0.4 mV, $n = 9$ cells from 3 mice, $P < 0.001$ vs. TASK-3 KO mice, Fig. 5*H–J*). One may argue that the less excitatory effect of NT on GCs in slices cut from TASK-3 KO mice assessed in whole-cell configuration may be due to the washout of the essential constituents required for the effect of NT. We therefore used perforated-patch recording method and replicated the experiments. In perforated-patch recording configuration, application of NT still induced a significantly smaller level of depolarization in slices cut from TASK-3 KO mice (1.2 ± 0.5 mV, $n = 9$ cells from 3 mice, $P < 0.001$ vs. baseline, Fig. 5*J*) than that from WT mice (5.1 ± 0.6 mV, $n = 10$ cells from 3 mice, $P < 0.001$ vs. TASK-3 KO mice, Fig. 5*J*) demonstrating that it is unlikely that NT-induced lower level of depolarization in TASK-3 KO mice was caused by washout of the essential constituents required for the effect of NT. However, in both recording configurations, application of NT still induced a small but significant depolarization in the slices cut from TASK-3 KO mice (Fig. 5*J*). One explanation is that NT may also modulate other channels, in addition to TASK-3 channels, to generate depolarization (see Discussion). However, these results together demonstrate that NT-induced depolarization in dentate gyrus GCs is mediated majorly by the inhibition of TASK-3 channels.

We further tested the interaction of NTS1 and TASK-3 channels by coexpressing NTS1 receptors and TASK-3 channels in HEK293 cells. Bath application of NT to HEK293 cells expressing NTS1 receptors and TASK-3 channels resulted in remarkable inhibition of the HCs recorded at −60 mV (−355.1 ± 84.9 pA, $n = 8$, $P = 0.004$, Fig. 5*K*). NT-induced currents had a reversal potential of −95.4 ± 3.4 mV ($n = 8$, Fig. 5*L*,*M*), which was close to the calculated K^+ reversal potential (−89.4 mV) in our recording condition suggesting that the activation of NTS1 receptors inhibits TASK-3 channel currents. As controls, the application of NT to HEK293 cells expressing either NTS1 receptors (−2.2 ± 11.5 pA, $n = 5$, $P = 0.86$, Fig. 5*N*) or TASK-3 channels (−7.8 ± 6.9 pA, $n = 5$, $P = 0.33$, Fig. 5*N*) alone failed to significantly alter the HCs further

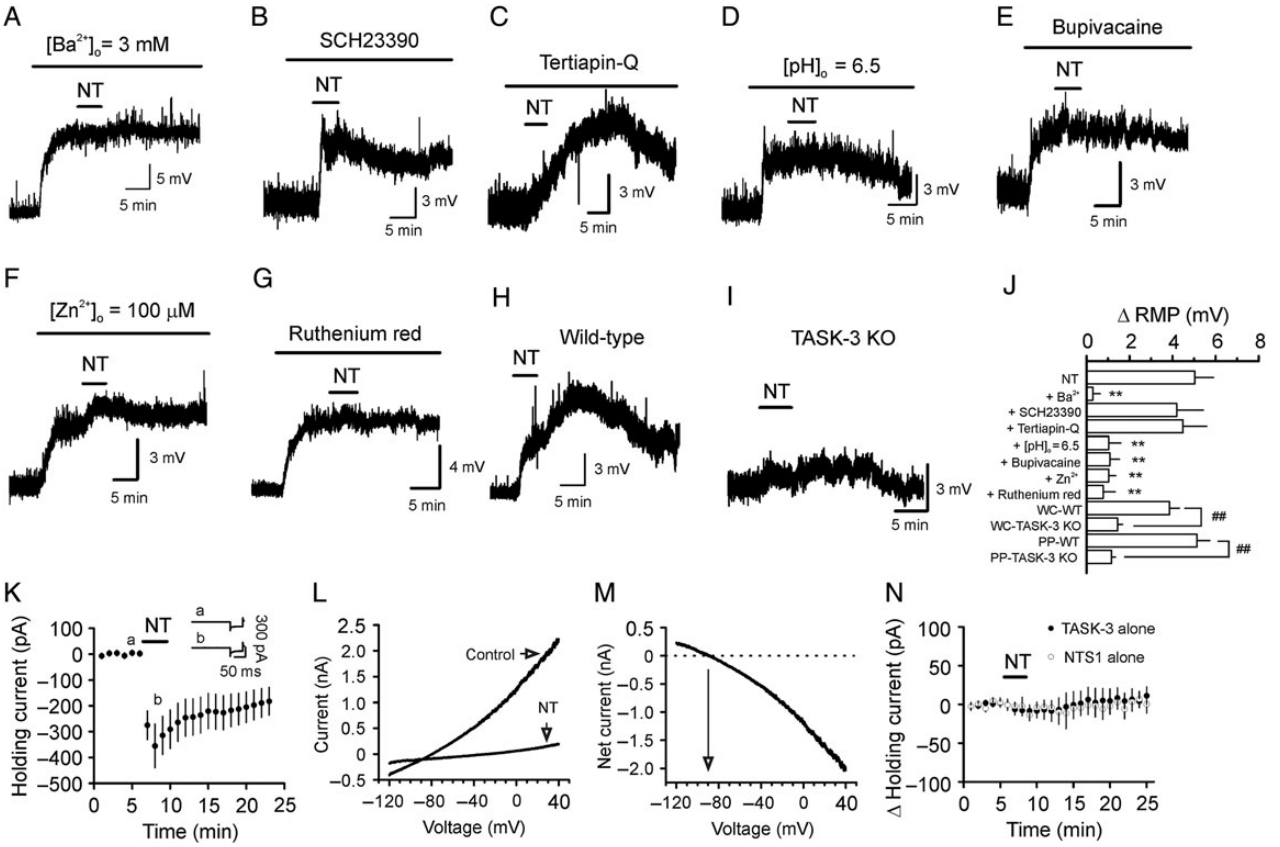

Figure 5. NT depolarizes the GCs by inhibiting TASK-3 channels. (*A*) Bath application of Ba^{2+} by itself induced membrane depolarization, and subsequent application of NT failed to further alter the membrane potential. (*B*) Application of SCH23390 (20 μM), a Kir inhibitor, failed to block NT-induced depolarization. (*C*) Application of tertiapin-Q (0.5 μM), another Kir inhibitor, failed to block NT-induced depolarization. (*D*) Lowering the extracellular solution pH from 7.4 to 6.5 induced a depolarization and blocked NT-induced depolarization. (*E*) Application of bupivacaine (200 μM), a TASK channel blocker, induced depolarization of the GCs and blocked NT-induced depolarization. (*F*) Inclusion of Zn^{2+} (100 μM), a TASK-3 channel blocker, in the extracellular solution produced depolarization and reduced NT-induced depolarization. (*G*) Inclusion of ruthenium red (10 μM), another TASK-3 channel blocker, in the extracellular solution depolarized the GCs and blocked NT-induced depolarization. (*H*) Bath application of NT depolarized the GCs in slices cut from WT mice. (*I*) Bath application of NT induced significantly smaller level of depolarization of the GCs in slices cut from TASK-3 KO mice. (*J*) Summary bar graph. WC-WT: whole-cell recording from slices cut from WT mice; WC-TASK-3 KO: whole-cell recording from slices cut from TASK-3 KO mice; PP-WT: perforated-patch recording from slices cut from WT mice; PP-TASK-3 KO: perforated-patch recording from slices cut from TASK-3 KO mice. (*K*) NT inhibited TASK-3 currents in HEK293 cells coexpressing NTS1 receptors and TASK-3 channels. (*L*) I–V curves recorded from a HEK293 cell coexpressing NTS1 and TASK-3 before and during the application of NT. (*M*) I–V curve of the net current generated by subtraction of the I–V curve before from that in the presence of NT. (*N*) Bath application of NT did not generate significant inward HCs in HEK293 cells expressing only NTS1 or TASK-3. $^{**}P < 0.01$ vs. NT alone; $^{\#\#}P < 0.01$.

supporting the inhibition of TASK-3 channels by NTS1 activation. These results together indicate that the activation of NTS1 receptors inhibits TASK-3 channels.

NT-Induced Depolarization may be Mediated by Direct Interaction of $G\alpha_{q/11}$ and TASK-3 Channels

We next probed the signaling mechanisms underlying NT-induced depolarization. Since NTS1 is a G protein-coupled receptor, we first tested the requirement of G proteins by including GDP-β-S (4 mM) in the recording pipettes. After formation of whole-cell configuration, we waited for ~20 min to allow the perfusion of GDP-β-S into the cells. Bath application of NT in the presence of GDP-β-S significantly reduced NT-induced depolarization (1.2 ± 0.5 mV, $n = 6$, $P = 0.005$ vs. NT alone, Fig. 6*A*,*H*) demonstrating that G proteins are required for NT-induced depolarization. We further tested the role of $G\alpha_{q/11}$ by applying a $G\alpha_{q/11}$ antibody via the recording pipettes. Application of $G\alpha_{q/11}$ antibody in this manner has been shown to inhibit the effects of $G\alpha_{q/11}$ on a variety of ion channels (Haley et al. 2000; Jin et al. 2002; Morita et al. 2002; Deng et al. 2006; Endoh 2006). Dialysis of $G\alpha_{q/11}$ antibody into the cells significantly inhibited NT-induced depolarization (20 μg/ml, 0.6 ± 0.9 mV, $n = 6$, $P = 0.005$, Fig. 6*B*,*H*), whereas infusion of Gβ antibody (20 μg/ml) in the same fashion failed to alter NT-mediated depolarization (3.9 ± 0.5 mV, $n = 7$, $P = 0.35$ vs. NT alone, data not shown). Because the activation of NTS1 increases the activity of PLC, we tested the roles of PLC in NT-induced depolarization. Application of U73122 (10 μM), a PLC inhibitor, failed to alter NT-induced depolarization (6.5 ± 1.1 mV, $n = 6$, $P = 0.31$, Fig. 6*C*,*H*) significantly. Furthermore, application of another PLC inhibitor, edelfosine (100 μM), did not significantly change NT-mediated depolarization (4.5 ± 0.8 mV, $n = 6$, $P = 0.65$, Fig. 6*D*,*H*). We next tested the roles of IP_3 receptors, intracellular Ca^{2+} and PKC. Intracellular application of the IP_3 receptor blocker, xestospongin C (5 μM), did not significantly influence NT-induced depolarization (4.8 ± 1.5 mV, $n = 6$, $P = 0.91$, Fig. 6*E*,*H*) suggesting that Ca^{2+} released from IP_3 store is unnecessary for NT-mediated depolarization. Application of BAPTA (10 mM) via the recording pipettes did not significantly change NT-mediated depolarization (4.3 ± 0.8 mV, $n = 7$, $P = 0.55$, Fig. 6*F*,*H*) suggesting that the effect of NT is independent of intracellular Ca^{2+} concentration. Furthermore, application of

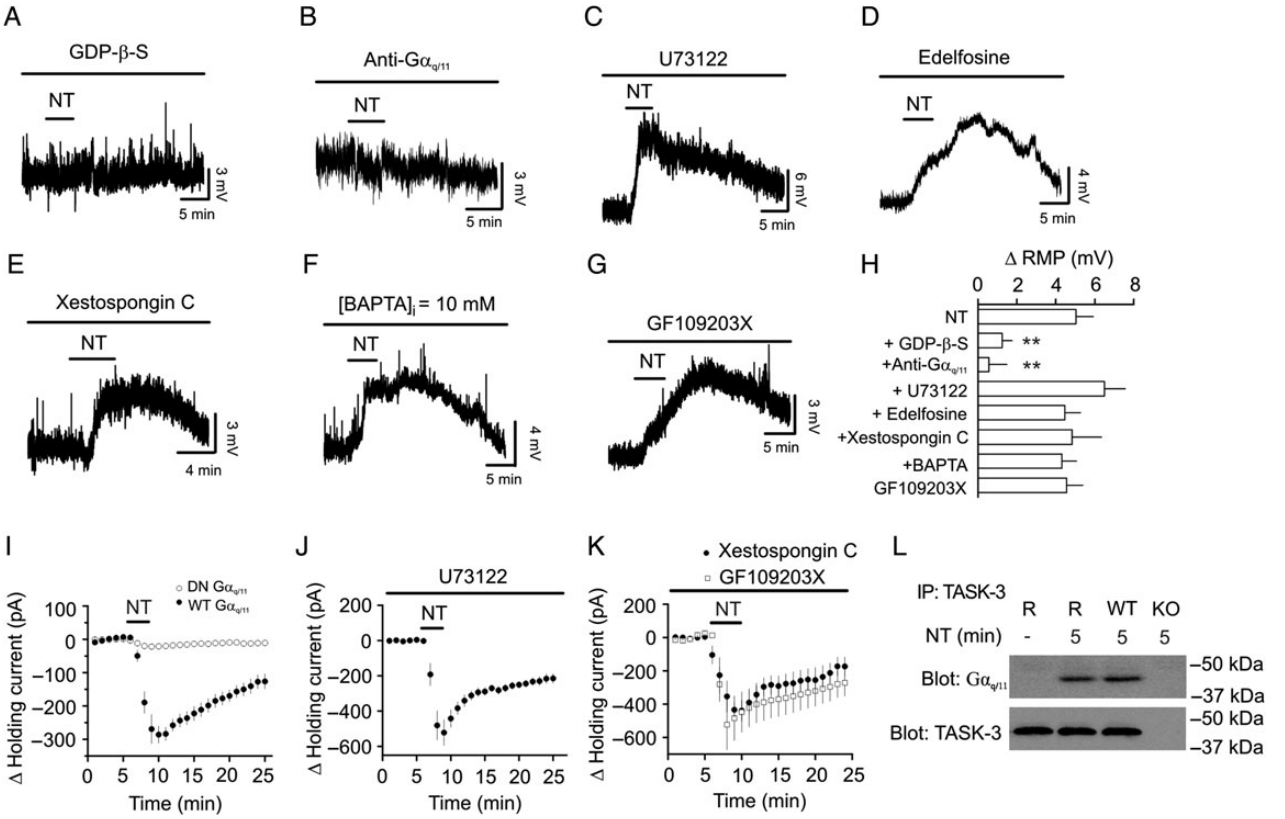

Figure 6. NT-mediated depolarization is mediated by direct coupling of $G\alpha_{q/11}$ to TASK-3 channels. (*A*) Inclusion of GDP-β-S in the recording pipettes blocked NT-induced depolarization. (*B*) Inclusion of anti-$G\alpha_{q/11}$ in the recording pipettes blocked NT-mediated depolarization. (*C*) Application of U73122, a PLC inhibitor, did not change NT-induced depolarization. (*D*) Application of edelfosine, another PLC inhibitor, did not block NT-induced depolarization. (*E*) Intracellular application of xestospongin C, a IP_3 receptor blocker, failed to block NT-induced depolarization. (*F*) Intracellular application of BAPTA did not change NT-mediated depolarization. (*G*) Application of GF109203X, a PKC inhibitor, did not alter NT-induced depolarization. (*H*) Summary bar graph. $^{**}P < 0.01$ vs. NT alone. (*I*) NT induced a significantly smaller inward HC in HEK293 cells co-transfected with NTS1, TASK-3, and DN-$G\alpha_{q/11}$ compared with those cells co-transfected with NTS1, TASK-3, and WT-$G\alpha_{q/11}$. (*J*) Application of U73122 did not change NT-induced increases in inward HCs in HEK293 cells coexpressing NTS1 and TASK-3. (*K*) Inclusion of xestospongin C in the recording pipettes or bath application of GF109203X did not alter NT-mediated increases in inward HCs in HEK293 cells transfected with NTS1 and TASK-3. (*L*) Association of $G\alpha_{q/11}$ with TASK-3 channels was detected in the lysate of the rat dentate gyrus immunoprecipitated with antibody to TASK-3 channels after the activation of NTS1. Rat dentate gyrus (denoted as R in the figure) was treated with or without NT for 5 min before being lysated. As a control, application of the same experimental procedures detected the association of $G\alpha_{q/11}$ with TASK-3 channels in the samples prepared from WT mice but not in those prepared from TASK-3 KO mice.

GF109203X (2 μM) failed to affect NT-induced depolarization significantly (4.6 ± 0.8 mV, $n = 7$, $P = 0.7$, Fig. 6*G*,*H*) suggesting that PKC is not required for NT-mediated depolarization in the GCs.

We further probed the signaling mechanisms underlying NT-induced depolarization in HEK293 cells co-transfected with NTS1 receptors and TASK-3 channels. Bath application of NT induced a significantly smaller HC in HEK293 cells coexpressing the dominant-negative $G\alpha_{q/11}$ (DN $G\alpha_{q/11}$), NTS1 receptors, and TASK-3 channels (–21.9 ± 5.9 pA, $n = 10$) compared with that in HEK293 cells co-transfected with the wild-type $G\alpha_{q/11}$ (WT $G\alpha_{q/11}$), NTS1 receptors, and TASK-3 channels (–285.8 ± 25.8 pA, $n = 7$, $P < 0.001$, Fig. 6*I*) demonstrating a necessary role of $G\alpha_{q/11}$. We further examined the roles of the downstream targets of G proteins. HEK293 cells were pre-incubated individually with the inhibitors for PLC (U73122, 10 μM), IP_3 receptors (xestospongin C, 1 μM), and PKC (GF109203X, 2 μM), and the same concentration of the inhibitors was applied in the bath. Under these circumstances, application of NT still induced comparable (vs. NT alone) inward HCs (U73122: –521.8 ± 73.9 pA, $n = 5$, $P = 0.2$, Fig. 6*J*; xestospongin C: –438.8 ± 63.4 pA, $n = 5$, $P = 0.5$, Fig. 6*K*; GF109203X: –523.0 ± 151.2 pA, $n = 6$, $P = 0.32$, Fig. 6*K*). We further corroborated the direct interaction of $G\alpha_{q/11}$ and TASK-3 channels mediating the NT-induced depolarization in the dentate gyrus using immunoprecipitation. After being treated with or without NT (0.5 μM) for 5 min, dentate gyrus slices were lysed and the lysates were immunoprecipitated with TASK-3 antibody. The immunoprecipitates were resolved by SDS–PAGE and western-blotted with $G\alpha_{q/11}$ antibody. As shown in Figure 6L, treatment of slices with NT for 5 min induced an association of the $G\alpha_{q/11}$ with the TASK-3 channels in rats. As a control, treatment of slices cut from WT mice with NT for 5 min induced the association of $G\alpha_{q/11}$ and TASK-3 channels, whereas no band was detected in the samples prepared from the TASK-3 KO mice with the same experimental procedures. These results demonstrate that NT-induced depolarization is mediated via direct interaction of $G\alpha_{q/11}$ with TASK-3 channels, as demonstrated previously (Chen et al. 2006; Mathie 2007; Veale et al. 2007).

Activation of NTS1 Receptors by Endogenously Released NT Enhances LTP at the PP-GC Synapses

We then probed the potential physiological function of NT-induced transient increase in the excitability of the GCs. We tested the hypothesis that NT-mediated transient depolarization of the

GCs modulates the induction and/or expression of LTP based on the results showing that the induction of LTP in the amygdala has been altered in NTS1 KO mice (Amano et al. 2008) and local release of NT is required for the D_1 dopamine receptor-mediated LTP at GABA synapses (Krawczyk et al. 2013). We tested the role of endogenously released NT in the induction and expression of LTP at the PP-GC synapses because the cell bodies of the PP in the entorhinal cortex express NT (Atoji et al. 1995) and numerous NT-immunoreactive varicose axons have been detected in the molecular layer of the dentate gyrus (Sakamoto et al. 1986), where the PP arrives. We first compared the level of LTPs in slices cut from WT and NTS1 KO mice. In slices cut from WT mice, high-frequency stimulation of the PP induced robust LTP (40 min after the induction protocol, 175 ± 12% of control, $n = 10$ cells from 4 mice, $P < 0.001$, Fig. 7A,F), whereas application of the same induction protocol to slices cut from NTS1 KO mice induced a significantly smaller LTP (40 min after the induction protocol, 127 ± 4% of control, $n = 14$ cells from 4 mice, $P < 0.0001$ vs. WT mice, two-way ANOVA, Fig. 7B,F). We further confirmed the role of NTS1 in LTP by inducing LTP in slices cut from WT mice in the presence of the NTS1 antagonist, SR48692. Slices were pretreated with 1 μM SR48692, and the same concentration of SR48692 was continuously applied in the bath. Under these circumstances, application of the high-frequency-stimulation induction protocol induced a significantly smaller LTP (132 ± 6% of control, $n = 10$ cells from 3 mice, $P = 0.001$ vs. LTP from WT mice without SR48692, two-way ANOVA, Fig. 7C,F) further supporting a role of NTS1 in LTP at the PP-GC synapses. The above-mentioned experimental results support a role of NTS1 in the expression of LTP. However, it is unclear whether the activation of NTS1 facilitates LTP by increasing the excitability of the GCs. Because the activation of NTS1 increased neuronal excitability by the inhibition of TASK-3 channels in the GCs and intracellular application of Cs^+-gluconate blocked NT-induced depolarization (Fig. 4I), we further tested the roles of NT-induced augmentation of neuronal excitability of the GCs in NT-mediated increase in LTP by using intracellular Cs^+-gluconate solution to block NT-induced depolarization. In slices cut from WT mice, application of the induction protocol induced a significantly smaller level of LTP (129 ± 11% of control, $n = 9$ from 3 WT mice, $P = 0.03$, Fig. 7D,F) compared with the LTP induced in the intracellular solution containing K^+-gluconate. We further tested the roles of TASK-3 channels in LTP at the PP-GC synapses. Application of the induction protocol induced a significantly smaller level of LTP in slices cut from TASK-3 KO mice (125 ± 8% of control, $n = 13$ from 3 mice, $P = 0.006$ vs. WT mice, Fig. 7E,F). These results demonstrate that NT-induced facilitation of the excitability of the GC facilitates LTP.

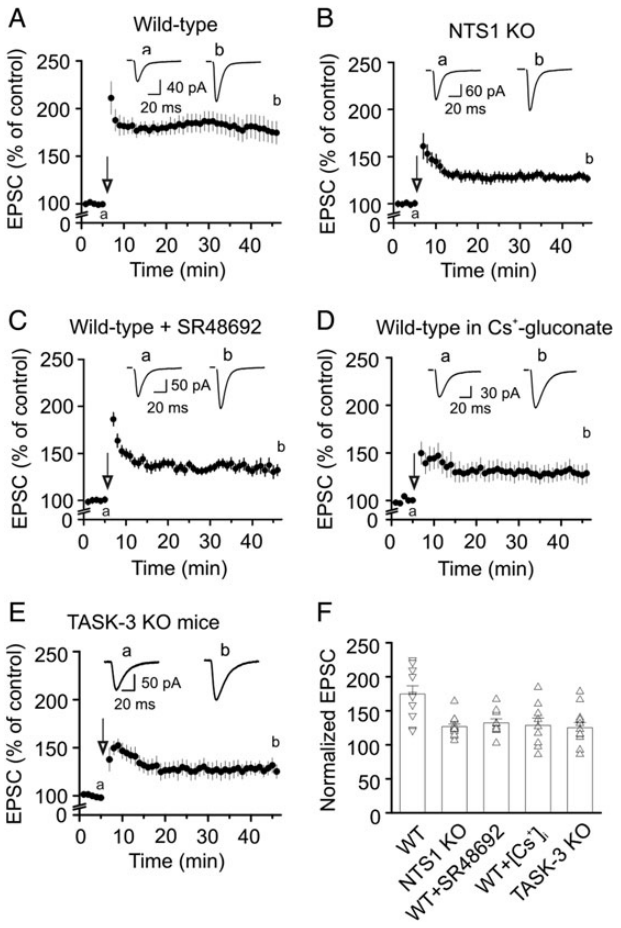

Figure 7. Endogenously released NT facilitates LTP at the PP-GC synapses. (*A*) Application of tetanic stimulation induced robust LTP at the PP-GC synapses in WT mice ($n = 10$ cells from 4 mice). Insets show the EPSCs recorded at the time points denoted in the figure. (*B*) Application of the same induction protocol induced a lower level of LTP at the PP-GC synapses in NTS1 KO mice ($n = 14$ cells from 3 mice). (*C*) Application of the same induction protocol induced a lower level of LTP in slices treated with the selective NTS1 antagonist, SR48692 (1 μM) in WT mice ($n = 10$ cells from 3 mice). (*D*) Application of the same induction protocol induced a lower level of LTP at the PP-GC synapses in slices ($n = 9$) cut from 3 WT mice when the pipette solution contained Cs^+-gluconate. (*E*) Application of the induction protocol induced a lower level of LTP at the PP-GC synapses in slices ($n = 13$) cut from 3 TASK-3 KO mice. (*F*) Summary graph showing LTP of individual cells and their average.

Discussion

Our results demonstrate that NT increases the neuronal excitability of dentate gyrus GCs via the activation of NTS1 receptors. Activation of NTS1 receptors depolarizes GCs by the inhibition of TASK-3 channels, and the signaling mechanisms may involve a direct coupling of $G\alpha_{q/11}$ and TASK-3 channels. NT-induced facilitation of neuronal excitability increases the level of LTP at the PP-GC synapses, further supporting a facilitatory role of NT in learning and memory.

Ionic Mechanisms Underlying NT-Induced Increase in Neuronal Excitability

Resting K^+ channels are the major determinants of neuronal membrane potential, and their inhibition is 1 of the principal mechanisms by which neurotransmitters or neuromodulators modulate neuronal excitability. Our results demonstrate that NT depolarizes GCs by inhibiting a resting K^+ conductance based on the following lines of experimental evidence. First, application of NT slightly but significantly increases the input resistance of the recorded cells suggesting that NT inhibits a membrane conductance. Second, replacement of extracellular NaCl with NMDG-Cl and depletion of extracellular Ca^{2+} failed to significantly change NT-induced depolarization suggesting that NT acts not by opening a cationic conductance. Third, replacing extracellular K^+ with the same concentration of Na^+ significantly enhanced NT-induced depolarization suggesting that the effect of NT is related to K^+ movement across the membrane. Although NT has been reported to inhibit Na^+/K^+ pump (Lopez Ordieres and Rodriguez de Lores Arnaiz 2000) and deprivation of extracellular K^+ should inactivate Na^+/K^+ pump, this result indicates that it is unlikely that NT-induced depolarization is mediated by the

inhibition of Na^+/K^+ pump. One explanation for NT-induced increase in depolarization in the absence of extracellular K^+ is that depletion of extracellular K^+ increases K^+ concentration gradient resulting in functional upregulation of basal K^+ channels and hence facilitates the inhibitory effect of NT on these channels. Fourth, substitution of intracellular K^+ with Cs^+ blocks NT-induced depolarization. Finally, NT-induced net currents have a reversal potential close to the calculated K^+ reversal potential, further demonstrating that NT depolarizes the GC by inhibiting a K^+ conductance.

We further identified the type of K^+ channels involved in NT-induced depolarization. Our results demonstrate that NT depolarizes the GCs by inhibiting TASK-3 channels based on the following array of evidence. First, TASK channels are sensitive to extracellular Ba^{2+}, and our results demonstrate that NT-induced depolarization is sensitive to Ba^{2+}. Although the Kirs are also sensitive to Ba^{2+}, our results show that it is unlikely that NT increases neuronal excitability in the GCs by inhibiting the Kirs because the I–V curve of NT-induced net currents does not show inward rectification and application of 2 Kir inhibitors (tertiapin-Q and SCH23390) do not block NT-mediated depolarization. Second, TASK channels are sensitive to acid and bupivacaine (Bayliss et al. 2003; Lesage 2003) and so is the NT-induced depolarization. Third, the NT-induced depolarization is sensitive to zinc and ruthenium red, 2 TASK-3 inhibitors, suggesting that NT increases neuronal excitability by inhibiting TASK-3 channels. Fourth, application of NT induces significantly smaller level of depolarization in the slices cut from TASK-3 KO mice than that from WT mice. Lastly, application of NT to HEK293 cells co-transfected with NTS1 receptors and TASK-3 channels induces remarkable inward HCs further supporting the involvement of TASK-3 channels. Consistent with our electrophysiological data, a high density of TASK-3 channels has been detected in the dentate gyrus GCs (Talley et al. 2001).

Whereas all the experimental evidence indicates that TASK-3 channels are the major targets for NT, there is still a possibility that other channels may have minor contribution to NT-mediated depolarization in dentate gyrus GCs because NT still generates a small depolarization (~1–1.5 mV) in TASK-3 KO mice with both whole-cell and perforated-patch recording methods (Fig. 5J). We propose 2 possibilities to explain the results. First, the small depolarization induced by NT in TASK-3 KO mice might be mediated by TASK-1 channels because these 2 types of channels share many biophysical properties such as that the I–V curve can be fit by GHK equation and pharmacological characteristics like being sensitive to pH and Ba^{2+}. TASK-1 and TASK-3 channels can also form heteromeric channels in neurons (Berg et al. 2004; Kang et al. 2004). Second, because we have shown previously that NT also inhibits TREK-2 channels in the entorhinal neurons to produce persistent depolarization (Xiao et al. 2014), a small contribution of TREK-2 channels to NT-induced depolarization in the dentate gyrus GCs cannot be excluded. However, the contribution of TREK-2 channels should be minimal because the IV curve of the net current generated by NT can be fit by GHK equation in contrast to the outward rectification of TREK-2 channels. Because the NT-induced remaining depolarization in the dentate gyrus GCs of TASK-3 KO mice is small and variable, it is difficult to further identify the underlying ion channels.

Signal Transduction Mechanisms Underlying NT-Induced Increase in Neuronal Excitability

Whereas NT interacts with 3 receptor types, our results demonstrate that NT-induced increases in neuronal excitability in the dentate gyrus GCs are mediated by the activation of NTS1 receptors because application of the selective NTS1 not NTS2 antagonist blocks the effect of NT on neuronal excitability. Furthermore, NT-induced augmentation of neuronal excitability is not observed in NTS1 KO mice but still exists in NTS2 KO mice. NTS1 receptors are G protein-coupled. Our results have demonstrated that the function of G proteins is required for NT-mediated depolarization. The result that dialysis of $G\alpha_{q/11}$ antibody into the cells blocked NT-induced membrane depolarization suggests that $G\alpha_{q/11}$ is required for NT-induced facilitation of neuronal excitability. However, our results do not support any roles of the intracellular molecules downstream of G-proteins in NT-induced depolarization. The principal intracellular pathway coupled to NTS1 receptors is PLC pathway that results in an increase in intracellular Ca^{2+} release and the activation of PKC. Nonetheless, our results indicate that this pathway is unlikely to be involved. One plausible explanation for our results is that NTS1 receptor activation releases $G\alpha_{q/11}$, which directly interacts with TASK-3 channels to enhance neuronal excitability. Our immunoprecipitation experiments further demonstrate that the activation of NTS1 receptors induces a physical association of $G\alpha_{q/11}$ and TASK-3 channels in the dentate gyrus. Consistent with our results is the observation that the activation of $G\alpha_q$-coupled receptors in a mammalian heterologous expression system results in depression of TASK channels via a direct $G\alpha_q$ coupling to TASK channels (Chen et al. 2006; Mathie 2007; Veale et al. 2007).

Whereas we failed to detect the roles of intracellular diffusable molecules such as PLC, IP_3 receptors and PKC in NT-induced inhibition of TASK-3 channels in the dentate gyrus GCs, the PKC and MAPK (ERK1/2) pathway is required for NT-induced depolarization in rat spinal cord dorsal horn neurons possibly by inhibiting TRESK or TASK-3 channels (Kadiri et al. 2011). Furthermore, the activation of PKC results in the inhibition of TASK-like, possibly TASK-3 channels in a rat nociceptive cell (Cooper et al. 2004). One possible explanation for the discrepancy of our results with those in the literature is that distinct neuronal environment or PKC isoforms may be responsible for the different results.

Roles of NT in LTP and Other Diseases

Whereas NT has been implicated in the modulation of a variety of physiological functions including pain, temperature, blood pressure, learning, and memory and neurological diseases such as schizophrenia and Parkinson's disease (Tyler-McMahon et al. 2000; Boules et al. 2013), the functional roles of NT-mediated increases in the excitability of the GCs have not been determined. In this study, we demonstrate that endogenously released NT increases the excitability of the GCs to facilitate the induction of LTP at the PP-GC synapses based on the following results. First, the level of LTP induced in slices cut from NTS1 KO mice was significantly lower than that induced in slices cut from WT mice. Second, application of the selective NTS1 antagonist, SR48692, significantly reduced the level of LTP in WT mice. Third, when the K^+-gluconate-containing intracellular solution was replaced with intracellular solution containing Cs^+-gluconate, the extent of LTP was significantly reduced in slices cut from WT mice. Fourth, the LTP level was significantly lower in TASK-3 KO mice compared with WT mice suggesting that NT-mediated inhibition of TASK-3 channels contributes to the induction of LTP. These results together support that NT-induced depolarization of the GCs facilitates the induction of LTP at the PP-GC synapses. Whereas our results demonstrate a facilitatory role of NTS1 in the induction of LTP at the PP-GC synapses, NTS1 receptors have been shown to exert an inhibitory role for the induction of LTP in the

basolateral nucleus of the amygdala (Amano et al. 2008). In this study, tetanic stimulation failed to reliably induce LTP in slices cut from WT mice whereas application of the same induction protocol induced pronounced LTP in slices cut from NTS1 KO mice and in slices cut from WT mice when NTS1 was pharmacologically blocked. The mechanism underlying NT-mediated modulation of LTP induction in the amygdala involves dopamine D_2 receptor-induced modulation of NMDA receptors (Amano et al. 2008). Whereas the mechanisms underlying NT-mediated facilitation of LTP at the PP-GC synapses require further exploration, it is unlikely that NT-mediated interaction of D_2 receptors with NMDA receptors plays a role at this synapse type because application of D_1- and D_2-like dopamine receptor blockers failed to block NT-induced increases in AP firing frequency (Fig. 2C). However, it is possible that NT-mediated depolarization of GCs facilitates the opening of NMDA receptors from Mg^{2+} blockade during the application of the induction protocol to facilitate LTP at the PP-GC synapses.

In conclusion, we have shown that the activation of NTS1 receptors in the dentate gyrus GCs increases neuronal excitability majorly by inhibiting TASk-3 channels. NT-mediated inhibition of TASK-3 channels is dependent on $G\alpha_{q/11}$ but does not require the functions of PLC, intracellular Ca^{2+} release and PKC, suggesting a direct coupling of $G\alpha_{q/11}$ with TASK-3 channels. Immunoprecipitation experiments further demonstrate that the activation of NTS1 receptors induces physical association of $G\alpha_{q/11}$ and TASK-3 channels in the dentate gyrus. NT-mediated increases in neuronal excitability facilitate the induction of LTP at the PP-GC synapses further supporting a role of NT in facilitating learning and memory.

Funding

This study was supported by National Institutes of Health (MH082881 to S.L. and NS33583 to D.A.B.).

Notes

Conflict of Interest: None declared.

References

Alexander MJ, Miller MA, Dorsa DM, Bullock BP, Melloni RH Jr, Dobner PR, Leeman SE. 1989. Distribution of neurotensin/neuromedin N mRNA in rat forebrain: unexpected abundance in hippocampus and subiculum. Proc Natl Acad Sci USA. 86: 5202–5206.

Aller MI, Veale EL, Linden AM, Sandu C, Schwaninger M, Evans LJ, Korpi ER, Mathie A, Wisden W, Brickley SG. 2005. Modifying the subunit composition of TASK channels alters the modulation of a leak conductance in cerebellar granule neurons. J Neurosci. 25:11455–11467.

Amano T, Wada E, Yamada D, Zushida K, Maeno H, Noda M, Wada K, Sekiguchi M. 2008. Heightened amygdala long-term potentiation in neurotensin receptor type-1 knockout mice. Neuropsychopharmacology. 33:3135–3145.

Ambrogini P, Lattanzi D, Ciuffoli S, Agostini D, Bertini L, Stocchi V, Santi S, Cuppini R. 2004. Morpho-functional characterization of neuronal cells at different stages of maturation in granule cell layer of adult rat dentate gyrus. Brain Res. 1017:21–31.

Atoji Y, Watanabe H, Yamamoto Y, Suzuki Y. 1995. Distribution of neurotensin-containing neurons in the central nervous system of the dog. J Comp Neurol. 353:67–88.

Azmi N, Norman C, Spicer CH, Bennett GW. 2006. Effects of a neurotensin analogue (PD149163) and antagonist (SR142948A) on the scopolamine-induced deficits in a novel object discrimination task. Behav Pharmacol. 17:357–362.

Bayliss DA, Sirois JE, Talley EM. 2003. The TASK family: two-pore domain background K^+ channels. Mol Interv. 3:205–219.

Berg AP, Talley EM, Manger JP, Bayliss DA. 2004. Motoneurons express heteromeric TWIK-related acid-sensitive K^+ (TASK) channels containing TASK-1 (KCNK3) and TASK-3 (KCNK9) subunits. J Neurosci. 24:6693–6702.

Boudin H, Lazaroff B, Bachelet CM, Pelaprat D, Rostene W, Beaudet A. 2000. Immunologic differentiation of two high-affinity neurotensin receptor isoforms in the developing rat brain. J Comp Neurol. 425:45–57.

Boules M, Li Z, Smith K, Fredrickson P, Richelson E. 2013. Diverse roles of neurotensin agonists in the central nervous system. Front Endocrinol (Lausanne). 4:36.

Bradford MM. 1976. A rapid and sensitive method for the quantitation of microgram quantities of protein utilizing the principle of protein-dye binding. Anal Biochem. 72:248–254.

Cadet JL, Kujirai K, Carlson E, Epstein CJ. 1993. Autoradiographic distribution of [^{3}H]neurotensin receptors in the brains of superoxide dismutase transgenic mice. Synapse. 14:24–33.

Carraway R, Leeman SE. 1973. The isolation of a new hypotensive peptide, neurotensin, from bovine hypothalami. J Biol Chem. 248:6854–6861.

Chen X, Talley EM, Patel N, Gomis A, McIntire WE, Dong B, Viana F, Garrison JC, Bayliss DA. 2006. Inhibition of a background potassium channel by Gq protein alpha-subunits. Proc Natl Acad Sci USA. 103:3422–3427.

Cooper BY, Johnson RD, Rau KK. 2004. Characterization and function of TWIK-related acid sensing K^+ channels in a rat nociceptive cell. Neuroscience. 129:209–224.

Deng PY, Lei S. 2007. Long-term depression in identified stellate neurons of juvenile rat entorhinal cortex. J Neurophysiol. 97:727–737.

Deng PY, Porter JE, Shin HS, Lei S. 2006. Thyrotropin-releasing hormone increases GABA release in rat hippocampus. J Physiol. 577:497–511.

Deng PY, Poudel SK, Rojanathammanee L, Porter JE, Lei S. 2007. Serotonin inhibits neuronal excitability by activating two-pore domain K^+ channels in the entorhinal cortex. Mol Pharmacol. 72:208–218.

Deng PY, Xiao Z, Jha A, Ramonet D, Matsui T, Leitges M, Shin HS, Porter JE, Geiger JD, Lei S. 2010. Cholecystokinin facilitates glutamate release by increasing the number of readily releasable vesicles and releasing probability. J Neurosci. 30:5136–5148.

Deng PY, Xiao Z, Yang C, Rojanathammanee L, Grisanti L, Watt J, Geiger JD, Liu R, Porter JE, Lei S. 2009. $GABA_B$ receptor activation inhibits neuronal excitability and spatial learning in the entorhinal cortex by activating TREK-2 K^+ channels. Neuron. 63:230–243.

Diaz-Cabiale Z, Fuxe K, Narvaez JA, Finetti S, Antonelli T, Tanganelli S, Ferraro L. 2002. Neurotensin-induced modulation of dopamine D_2 receptors and their function in rat striatum: counteraction by a NTR1-like receptor antagonist. Neuroreport. 13:763–766.

Endoh T. 2006. Dual effects of neurokinin on calcium channel currents and signal pathways in neonatal rat nucleus tractus solitarius. Brain Res. 1110:116–127.

Faggin BM, Zubieta JK, Rezvani AH, Cubeddu LX. 1990. Neurotensin-induced dopamine release in vivo and in vitro from substantia nigra and nucleus caudate. J Pharmacol Exp Ther. 252:817–825.

Ferraro L, O'Connor WT, Antonelli T, Fuxe K, Tanganelli S. 1997. Differential effects of intrastriatal neurotensin(1-13) and neurotensin(8-13) on striatal dopamine and pallidal GABA release. A dual-probe microdialysis study in the awake rat. Eur J Neurosci. 9:1838–1846.

Haley JE, Delmas P, Offermanns S, Abogadie FC, Simon MI, Buckley NJ, Brown DA. 2000. Muscarinic inhibition of calcium current and M current in Gαq-deficient mice. J Neurosci. 20:3973–3979.

Hermans E, Maloteaux JM. 1998. Mechanisms of regulation of neurotensin receptors. Pharmacol Ther. 79:89–104.

Heurteaux C, Guy N, Laigle C, Blondeau N, Duprat F, Mazzuca M, Lang-Lazdunski L, Widmann C, Zanzouri M, Romey G, et al. 2004. TREK-1, a K^+ channel involved in neuroprotection and general anesthesia. EMBO J. 23:2684–2695.

Hwang JI, Kim DK, Kwon HB, Vaudry H, Seong JY. 2009. Phylogenetic history, pharmacological features, and signal transduction of neurotensin receptors in vertebrates. Ann N Y Acad Sci. 1163:169–178.

Jin X, Morsy N, Shoeb F, Zavzavadjian J, Akbarali HI. 2002. Coupling of M_2 muscarinic receptor to L-type Ca channel via c-src kinase in rabbit colonic circular smooth muscle. Gastroenterology. 123:827–834.

Kadiri N, Rodeau JL, Schlichter R, Hugel S. 2011. Neurotensin inhibits background K^+ channels and facilitates glutamatergic transmission in rat spinal cord dorsal horn. Eur J Neurosci. 34:1230–1240.

Kang D, Han J, Talley EM, Bayliss DA, Kim D. 2004. Functional expression of TASK-1/TASK-3 heteromers in cerebellar granule cells. J Physiol. 554:64–77.

Kohler C, Radesater AC, Chan-Palay V. 1987. Distribution of neurotensin receptors in the primate hippocampal region: a quantitative autoradiographic study in the monkey and the postmortem human brain. Neurosci Lett. 76:145–150.

Kohler C, Radesater AC, Hall H, Winblad B. 1985. Autoradiographic localization of [^{3}H]neurotensin-binding sites in the hippocampal region of the rat and primate brain. Neuroscience. 16:577–587.

Krawczyk M, Mason X, Debacker J, Sharma R, Normandeau CP, Hawken ER, Di Prospero C, Chiang C, Martinez A, Jones AA, et al. 2013. D_1 dopamine receptor-mediated LTP at GABA synapses encodes motivation to self-administer cocaine in rats. J Neurosci. 33:11960–11971.

Kuzhikandathil EV, Oxford GS. 2002. Classic D_1 dopamine receptor antagonist R-(+)-7-chloro-8-hydroxy-3-methyl-1-phenyl-2,3,4,5-tetrahydro-1H-3-benzazepine hydrochloride (SCH23390) directly inhibits G protein-coupled inwardly rectifying potassium channels. Mol Pharmacol. 62:119–126.

Lapchak PA, Araujo DM, Quirion R, Beaudet A. 1990. Neurotensin regulation of endogenous acetylcholine release from rat cerebral cortex: effect of quinolinic acid lesions of the basal forebrain. J Neurochem. 55:1397–1403.

Lapchak PA, Araujo DM, Quirion R, Beaudet A. 1991. Neurotensin regulation of endogenous acetylcholine release from rat striatal slices is independent of dopaminergic tone. J Neurochem. 56:651–657.

Laszlo K, Toth K, Kertes E, Peczely L, Ollmann T, Lenard L. 2010. Effects of neurotensin in amygdaloid spatial learning mechanisms. Behav Brain Res. 210:280–283.

Lazarenko RM, Willcox SC, Shu S, Berg AP, Jevtovic-Todorovic V, Talley EM, Chen X, Bayliss DA. 2010. Motoneuronal TASK channels contribute to immobilizing effects of inhalational general anesthetics. J Neurosci. 30:7691–7704.

Lesage F. 2003. Pharmacology of neuronal background potassium channels. Neuropharmacology. 44:1–7.

Li J, Chen C, He Q, Li H, Moyzis RK, Xue G, Dong Q. 2011. Neurotensin receptor 1 gene (NTSR1) polymorphism is associated with working memory. PLoS One. 6:e17365.

Li S, Geiger JD, Lei S. 2008. Neurotensin enhances GABAergic activity in rat hippocampus CA1 region by modulating L-type calcium channels. J Neurophysiol. 99:2134–2143.

Lopez Ordieres MG, Rodriguez de Lores Arnaiz G. 2000. Neurotensin inhibits neuronal Na^+,K^+-ATPase activity through high affinity peptide receptor. Peptides. 21:571–576.

Lotstra F, Mailleux P, Schiffmann SN, Vierendeels G, Vanderhaeghen JJ. 1989. Neurotensin containing neurones in the human hippocampus of the adult and during development. Neurochem Int. 14:143–151.

Maeno H, Yamada K, Santo-Yamada Y, Aoki K, Sun YJ, Sato E, Fukushima T, Ogura H, Araki T, Kamichi S, et al. 2004. Comparison of mice deficient in the high- or low-affinity neurotensin receptors, Ntsr1 or Ntsr2, reveals a novel function for Ntsr2 in thermal nociception. Brain Res. 998:122–129.

Mathie A. 2007. Neuronal two-pore-domain potassium channels and their regulation by G protein-coupled receptors. J Physiol. 578:377–385.

Mazella J. 2001. Sortilin/neurotensin receptor-3: a new tool to investigate neurotensin signaling and cellular trafficking? Cell Signal. 13:1–6.

Mazella J, Botto JM, Guillemare E, Coppola T, Sarret P, Vincent JP. 1996. Structure, functional expression, and cerebral localization of the levocabastine-sensitive neurotensin/neuromedin N receptor from mouse brain. J Neurosci. 16:5613–5620.

Mazella J, Zsurger N, Navarro V, Chabry J, Kaghad M, Caput D, Ferrara P, Vita N, Gully D, Maffrand JP, et al. 1998. The 100-kDa neurotensin receptor is gp95/sortilin, a non-G-protein-coupled receptor. J Biol Chem. 273:26273–26276.

Morita H, Sharada T, Takewaki T, Ito Y, Inoue R. 2002. Multiple regulation by external ATP of nifedipine-insensitive, high voltage-activated Ca^{2+} current in guinea-pig mesenteric terminal arteriole. J Physiol. 539:805–816.

Moyse E, Rostene W, Vial M, Leonard K, Mazella J, Kitabgi P, Vincent JP, Beaudet A. 1987. Distribution of neurotensin binding sites in rat brain: a light microscopic radioautographic study using monoiodo [^{125}I]Tyr3-neurotensin. Neuroscience. 22:525–536.

Navarro V, Martin S, Sarret P, Nielsen MS, Petersen CM, Vincent J, Mazella J. 2001. Pharmacological properties of the mouse neurotensin receptor 3. Maintenance of cell surface receptor during internalization of neurotensin. FEBS Lett. 495:100–105.

Nouel D, Sarret P, Vincent JP, Mazella J, Beaudet A. 1999. Pharmacological, molecular and functional characterization of glial neurotensin receptors. Neuroscience. 94:1189–1197.

O'Connor WT, Tanganelli S, Ungerstedt U, Fuxe K. 1992. The effects of neurotensin on GABA and acetylcholine release in the dorsal striatum of the rat: an in vivo microdialysis study. Brain Res. 573:209–216.

Ohinata K, Sonoda S, Inoue N, Yamauchi R, Wada K, Yoshikawa M. 2007. Beta-lactotensin, a neurotensin agonist peptide derived from bovine beta-lactoglobulin, enhances memory consolidation in mice. Peptides. 28:1470–1474.

Pelaprat D. 2006. Interactions between neurotensin receptors and G proteins. Peptides. 27:2476–2487.

Petkova-Kirova P, Rakovska A, Della Corte L, Zaekova G, Radomirov R, Mayer A. 2008. Neurotensin modulation of acetylcholine, GABA, and aspartate release from rat prefrontal

cortex studied in vivo with microdialysis. Brain Res Bull. 77:129–135.

Quirion R, Welner S, Gauthier S, Bedard P. 1987. Neurotensin receptor binding sites in monkey and human brain: autoradiographic distribution and effects of 1-methyl-4-phenyl-1,2,3,6-tetrahydropyridine treatment. Synapse. 1:559–566.

Rakovska A, Giovannini MG, Della Corte L, Kalfin R, Bianchi L, Pepeu G. 1998. Neurotensin modulation of acetylcholine and GABA release from the rat hippocampus: an in vivo microdialysis study. Neurochem Int. 33:335–340.

Ramanathan G, Cilz NI, Kurada L, Hu B, Wang X, Lei S. 2012. Vasopressin facilitates GABAergic transmission in rat hippocampus via activation of V_{1A} receptors. Neuropharmacology. 63:1218–1226.

Reyneke L, Russell VA, Taljaard JJ. 1992. Regional effects of neurotensin on the electrically stimulated release of [^{3}H]dopamine and [^{14}C]acetylcholine in the rat nucleus accumbens. Neurochem Res. 17:1143–1146.

Roberts GW, Crow TJ, Polak JM. 1981. Neurotensin: first report of a cortical pathway. Peptides. 2(Suppl 1):37–43.

Rowe WB, Kar S, Meaney MJ, Quirion R. 2006. Neurotensin receptor levels as a function of brain aging and cognitive performance in the Morris water maze task in the rat. Peptides. 27:2415–2423.

Sakamoto N, Michel JP, Kiyama H, Tohyama M, Kopp N, Pearson J. 1986. Neurotensin immunoreactivity in the human cingulate gyrus, hippocampal subiculum and mammillary bodies. Its potential role in memory processing. Brain Res. 375:351–356.

Sarret P, Gendron L, Kilian P, Nguyen HM, Gallo-Payet N, Payet MD, Beaudet A. 2002. Pharmacology and functional properties of NTS2 neurotensin receptors in cerebellar granule cells. J Biol Chem. 277:36233–36243.

St-Gelais F, Jomphe C, Trudeau LE. 2006. The role of neurotensin in central nervous system pathophysiology: what is the evidence? J Psychiatry Neurosci. 31:229–245.

Talley EM, Solorzano G, Lei Q, Kim D, Bayliss DA. 2001. Cns distribution of members of the two-pore-domain (KCNK) potassium channel family. J Neurosci. 21:7491–7505.

Tirado-Santiago G, Lazaro-Munoz G, Rodriguez-Gonzalez V, Maldonado-Vlaar CS. 2006. Microinfusions of neurotensin antagonist SR 48692 within the nucleus accumbens core impair spatial learning in rats. Behav Neurosci. 120:1093–1102.

Tyler-McMahon BM, Boules M, Richelson E. 2000. Neurotensin: peptide for the next millennium. Regul Pept. 93:125–136.

Veale EL, Kennard LE, Sutton GL, MacKenzie G, Sandu C, Mathie A. 2007. Gαq-mediated regulation of TASK3 two-pore domain potassium channels: the role of protein kinase C. Mol Pharmacol. 71:1666–1675.

Vincent JP, Mazella J, Kitabgi P. 1999. Neurotensin and neurotensin receptors. Trends Pharmacol Sci. 20:302–309.

von Euler G, Fuxe K, Benfenati F, Hansson T, Agnati LF, Gustafsson JA. 1989. Neurotensin modulates the binding characteristics of dopamine D_2 receptors in rat striatal membranes also following treatment with toluene. Acta Physiol Scand. 135:443–448.

Wang S, Chen X, Kurada L, Huang Z, Lei S. 2012. Activation of group II metabotropic glutamate receptors inhibits glutamatergic transmission in the rat entorhinal cortex via reduction of glutamate release probability. Cereb Cortex. 22:584–594.

Wang S, Zhang AP, Kurada L, Matsui T, Lei S. 2011. Cholecystokinin facilitates neuronal excitability in the entorhinal cortex via activation of TRPC-like channels. J Neurophysiol. 106:1515–1524.

Watson MA, Yamada M, Cusack B, Veverka K, Bolden-Watson C, Richelson E. 1992. The rat neurotensin receptor expressed in Chinese hamster ovary cells mediates the release of inositol phosphates. J Neurochem. 59:1967–1970.

Xiao Z, Cilz NI, Kurada L, Hu B, Yang C, Wada E, Combs CK, Porter JE, Lesage F, Lei S. 2014. Activation of neurotensin receptor 1 facilitates neuronal excitability and spatial learning and memory in the entorhinal cortex: beneficial actions in an Alzheimer's disease model. J Neurosci. 34:7027–7042.

Xiao Z, Deng PY, Rojanathammanee L, Yang C, Grisanti L, Permpoonputtana K, Weinshenker D, Doze VA, Porter JE, Lei S. 2009. Noradrenergic depression of neuronal excitability in the entorhinal cortex via activation of TREK-2 K^+ channels. J Biol Chem. 284:10980–10991.

Yamauchi R, Wada E, Kamichi S, Yamada D, Maeno H, Delawary M, Nakazawa T, Yamamoto T, Wada K. 2007. Neurotensin type 2 receptor is involved in fear memory in mice. J Neurochem. 102:1669–1676.

Yin HH, Adermark L, Lovinger DM. 2008. Neurotensin reduces glutamatergic transmission in the dorsolateral striatum via retrograde endocannabinoid signaling. Neuropharmacology. 54:79–86.